with the possible exception of a single dacite. Possible triggers for melting may include: breakdown of hydrous phases during lithospheric thickening; hydration of the mantle lithosphere by underthrusting of the Arabian passive margin; small-scale edge-driven convection due to a significant thickness gradient in the Zagros lithosphere. Such processes may account for small-volume syn-collisional mantle-derived magmatism elsewhere in regions of thick lithosphere where recent slab break-off or lithospheric delamination cannot be proven.

1. Introduction

Magmatism is an important aspect of the Arabia-Eurasia collision, tens of millions of years after the initial docking of the two continental margins: dozens of centres have been active in the Pliocene-Quaternary, from eastern Turkey to eastern Iran (Fig. 1a; e.g. Pearce et al., 1990; Notsu et al., 1995; Keskin et al., 1998; Kheirkhah et al., 2009; Dilek et al., 2010; Saadat and Stern, 2012). Data are rapidly emerging on the chemistry of these rocks, which, together with other geological and geophysical constraints, tells us about the evolution of the young continental lithosphere. It is clear that they are compositionally diverse: the reported chemistries range from OIB-like (Walker et al., 2009; Pang et al., 2012), to calc-alkaline (Pearce et al., 1990), to potassic/ultrapotassic (Ahmadzadeh et al., 2010). Silicic adakite-like compositions have been reported from felsic intrusive rocks (Jahangiri 2007; Omrani et al., 2008), the significance of which is not entirely clear.

In this paper we present new elemental and isotopic whole-rock data from a previously unanalysed centre near Mahabad, in West Azerbaijan Province, NW Iran. Part of the aim of this study is to fill in a missing piece of the jigsaw: the Mahabad centre lies geographically between recently-reported centres to the north and southeast (Kheirkhah et al., 2009; Allen et al., 2013). A more generic aim is to use the Mahabad compositions, which are unusually basic for the Arabia-Eurasia collision and collision zone magmatism in general, to infer conditions and triggers for melting in the late Cenozoic collision zone.

2. Geological setting and nature of the samples

2.1. Regional geology and structure

Our samples are from lavas that were erupted over the Sanandaj-Sirjan Zone, which is regarded as one of the basement blocks of Iran (Fig. 1b). The Sanandaj-Sirjan Zone and other Iranian crustal blocks represent micro-continents derived from Gondwana, that collided with each other and with Eurasia during the Mesozoic as part of the evolution and eventual elimination of the Tethyan Ocean (Şengör et al., 1988). The Eocene, and perhaps especially the Middle Eocene, was a time of intensified magmatic activity within southwest Eurasia. The compositions of these rocks are typically calc-alkaline, and the magmatism is interpreted as an example of arc and back-arc volcanism in an extensional, pre-collisional setting (Vincent et al., 2005; Verdel et al., 2011). The magmatic front is commonly taken as the southwestern edge of the Urumieh-Dokhtar Zone, which runs NW-SE along the length of Iran (Fig. 1b). The northeastern boundary of the Sanandaj-Sirjan Zone is taken as this line, implying that it is also a lithospheric-scale suture with the next microcontinental basement block to the north. However, Eocene and Paleocene magmatism is present within the Sanandaj-Sirjan Zone itself (Mazhari et al., 2009), so that this distinction is not clear-cut.

The Arabia-Eurasia collision is the largest and most recent Tethyan orogen in southwest Asia; the Arabia-Eurasia suture lies ~60 km southwest of the studied rocks (Fig. 1c), making them some of the lavas erupted closest to the suture in the late Cenozoic. Initial Arabia-Eurasia collision began tens of millions of years ago. Although the age is debated, most estimates put initial collision in the 35-20 Ma range (e.g. Allen and Armstrong, 2008; Okay et al., 2010; McQuarrie and van Hinsbergen, 2013). The reduction in magmatic production by the end of the Eocene certainly implies some major tectonic reconfiguration at ~35 Ma. Regardless of the precise time of initial collision, convergence has continued to the present (McQuarrie et al., 2003). Current GPS-derived convergence rates are roughly 20 mm/yr at the longitude of the study area (Vernant et al., 2004), while Iran, Turkey, Armenia and neighbouring countries have a history of strong, frequent and tragic seismicity.

Active strain is not distributed evenly across the collision zone (Jackson et al., 1995). The Mahabad lavas and the Sanandaj-Sirjan Zone as a whole presently lie within the Turkish-Iranian Plateau. This area covers ~1.5 million km^2, roughly half of the total area deformed by the collision. It is marked by high elevations (typically 1.5 – 2 km) and low relief compared with mountains ranges to the south and north where convergent deformation is more active (e.g. Zagros, Alborz, Kopeh Dagh and Greater Caucasus ranges). Current deformation rates can be gauged from seismicity and the GPS-derived velocity field: they are modest (Jackson et al., 1995; Vernant et al., 2004), and internal deformation across the plateau proceeds at < 2 mm/yr. However, there is evidence for a faster rate of late Cenozoic deformation, comprising both shortening/thickening of the crust by thrusts and strike-slip faulting (Morley et al., 2009; Allen et al., 2011a). The Turkish-Iranian Plateau is also notable for its magmatism: there appears to have been a surge in volcanic activity in the Late Miocene-Quaternary, compared with the preceding 20-30 million years (e.g. Yilmaz et al., 1998; Davidson et al., 2004; Shabanian et al., 2012). Many of the Quaternary centres are in regions which have otherwise experienced little or no magmatism since the Eocene.

The reasons for this recent magmatism are not clear, and a variety of mechanisms have been proposed. Pearce et al. (1990) suggested delamination of the lithosphere in the collision zone, in line with equivalent hypotheses for the generation of collisional magmatism in Tibet (e.g. Chung et al., 2005). Keskin (2003) proposed break-off of the subducted Tethyan oceanic slab as the trigger. Both of these studies focussed on the magmatism in eastern Anatolia (Fig. 1), which is a region with unusually thin mantle lithosphere (~20 km or less), beneath crust that is ~40 km thick (Angus et al., 2006; Zor et al., 2008). Such mechanisms are hard to apply further east in the collision zone, where both crustal and overall lithospheric thicknesses are much higher. Mahabad lies above crust approximately 45-50 km thick, thicker

than much of Eastern Anatolia (Zor et al., 2003). The regional depth of the lithosphere-asthenosphere boundary has been estimated from modelling of shear wave velocities by Priestley et al. (2012), giving a lithospheric thickness of at least 140 km for Mahabad. The erupted lavas also lie above a significant gradient between lithosphere of near 250 km thickness at the core of the Zagros to the southeast, and <100 km to the north (Angus et al., 2006). The vertical resolution of the Priestley et al. (2012) study is ±30 km (Fig. 1c).

2.2. Field geology

Lavas are mapped as Quaternary (Eftekhar-Nezhad, 1973), but no radiometric ages are available. The Quaternary assignment is consistent with the fresh, undeformed appearance of the flows above all other strata in the area, and with published Quaternary ages for the closest centres to the north and south (Boccaletti et al., 1976; Allen et al., 2011b).

The analysed samples are from flows that overlie the limestones, clastics, and marls of the Qom formation (Miocene) or Jurassic to Cretaceous marine shales intercalated with limestones and volcanic rocks (Eftekhar-Nezhad, 1973). Samples were collected from close to the Bukan-Mahabad road, approximately 20-30 km southeast of Mahabad (Fig. 2). The only felsic sample analysed (M1.1) is from the summit of Kuh-e-Sultan, an incised rhyolite outcrop rising around 300 m above the surrounding topography north of the road. The rock is fresh, medium-grained and leucocratic, and contains flow textures. Some of the mafic samples, ranging from basanites to nephelinite (M2.1, 2.3, 2.4, 3.1, 3.2, 4.2), were collected from lava flows either side of the Bukan-Mahabad road just southeast of the village of Borhan. The rest (M5.2, 6.1, 7.1) were basanites and alkali basalts collected from the southeast of Isākandi village. The flows themselves reach up to 15 meters thick, thickening towards the southwest, and are commonly columnar-jointed.

2.3. Petrography

Nine mafic samples along with a single felsic sample were analysed in this study, with a total of five subjected to Nd-Sr isotope analysis. The list of samples, including GPS co-ordinates, is presented in Supplementary Item A1. The least evolved mafic samples (mostly basanites; see Section 4.1) are fine-grained clinopyroxene- and olivine-phyric lavas, with euhedral or slightly rounded phenocrysts reaching 2-3 mm. Some of the olivines have dark brown iddingsite rims. The groundmass consists of small olivines and clinopyroxenes, or devitrified glass, alongside abundant oxides, with some vesicles containing zeolite infill. More evolved samples (alkali basalts; Section 4.1) contain less olivine than the basanites, and tend to have a glomeroporphyritic texture dominated by clots of clinopyroxene. They have a fine-grained groundmass with conspicuous acicular clinopyroxene and nepheline crystals. Aside from occasional altered glass and zeolite infill, the lavas are fresh, and the mafic samples do not appear to contain hydrous phases with the exception of a small proportion of hornblende replacing clinopyroxene. The felsic sample is a medium-grained intrusive dacite dominated by quartz and feldspars with <5% hornblende, and rare cm-scale xenoliths of a finer-grained rock of a similar composition – possibly an earlier quickly cooled dacite magma that was broken up by later injections. Overall the texture is porphyritic, with phenocrysts of plagioclase reaching a maximum of 1 cm diameter, and rare hornblende and biotite; accessory phases include titanite and apatite.

3. Analytical Methods

Analytical methods are largely as reported in Neill et al. (in review) and reproduced here. Whole-rock samples were powdered by agate ball mill at Durham University. Major

element analysis was conducted on fused glass beads using a PANalytical Axios Advanced X-Ray Fluorescence (XRF) spectrometer at the University of Leicester. Leftover fractions not used for XRF analysis were digested using a standard HF and HNO_3 technique prior to trace element analysis. Solutions were run on a Thermo X2 inductively-coupled plasma mass spectrometer (ICP-MS) at the Northern Centre for Isotopic and Elemental Tracing (NCIET) at Durham University. Accuracy, precision, and reproducibility were monitored using blanks, multi-run and within-run duplicates, Re-Rh spike solutions, and five international reference standards. Standard W2 (n = 15) gave first relative standard deviations of 5% or better for most transition metals (excepting 10% for Sc, 12% for Cr, 6% for Ni), the large ion lithophile elements (LILE), high field strength elements (HFSE) and the rare earth elements (REE) (excepting 7% for La, 6% for Ce). Results are presented in Table 1.

Whole-rock radiogenic Nd-Sr isotope analysis was conducted at NCIET, with column chemistry for elemental pre-concentration based on the method of Dowall et al. (2007). Powders were digested in HF and HNO_3, and solutions were run through 1 ml pipette tips containing several drops of dilute Sr-spec resin to collect the Sr-bearing fraction. The high field strength element (HFSE)- and rare earth element (REE)-bearing fraction from these columns was run through 10 ml Bio-Rad polypropylene columns containing 1 ml of Bio-Rad AG1-X8 200-400 mesh anion-exchange resin. Neodymium was collected as part of a general rare earth element fraction. Analysis was conducted on a Thermo Neptune Mass Collector ICP-MS. Strontium blanks averaged 88 pg (n = 6). International reference standard NBS987 gave a mean of $^{87}Sr/^{86}Sr = 0.710263 \pm 0.000012$ (2σ, n = 12), comparable to a preferred value of 0.710240, and providing a minimum uncertainty of 16 ppm (2σ). Neodymium blanks averaged 10 pg (n = 6). A combination of the J&M standard and a Sm-doped version gave a mean $^{143}Nd/^{144}Nd = 0.511098 \pm 0.000007$ (2σ, n = 13), and a minimum uncertainty of 13 ppm

(2σ). Results are normalised relative to a preferred value of 0.511110, and are presented in Table 2.

4. Results

4.1. Alteration and elemental mobility

All of the samples have LOI values of <2.6 wt.% (Table 1), low enough to imply these rocks have not undergone significant alteration, and that thus most elemental concentrations, including the mobile alkalis and LILE (Pearce et al., 1996) are reflective of the original magma. In thin section, we have already noted that the samples are not obviously altered except for a few scattered patches that appear slightly oxidised. The presence of iddingsite aside, there is no evidence for large-scale alteration of the mafic minerals in, for example, the occurrence of serpentine, talc, and/or chlorite. $^{87}Sr/^{86}Sr$ ratios are extremely sensitive to alteration processes, but are depleted relative to Bulk Earth and show no systematic variation in relation to LOI (Table 2).

4.2. Major element geochemistry

The mafic rocks split into two categories, as seen on the total alkali-silica plot (Fig. 3). The samples which contain 41-42 wt.% SiO_2 plot mostly as basanites with significant silica under-saturation. They contain 13 wt.% Al_2O_3, 11-12 wt.% MgO, and 13-15 wt.% CaO; with the least siliceous sample falling just into the nephelinite field (M2.4). These samples are among the most basic recorded from the young centres of the Arabia-Eurasia collision zone. In spite of modestly abundant phenocrysts in these samples, they do not have obvious cumulate textures. Two samples (M6.1 and M7.1) are less alkaline, and plot as alkali basalts,

with 47 wt.% SiO_2, 15 wt.% Al_2O_3, 7-8 wt.% MgO, and 11 wt.% CaO (Table 1). Modal Mg# ranges from around 70 in the basanites and nephelinite to 60 in the alkali basalts. The basanites are extremely sodic (Na_2O/K_2O = 7-15, <0.5 wt.% K_2O), apart from M2.4, the nephelinite, which is more considerably more potassic (Na_2O/K_2O = 1.5, K_2O = 1.8 wt.%). The alkali basalts have similar total alkali concentrations and ratios to the nephelinite and may be classed as shoshonites on the K_2O vs. SiO_2 diagram (Fig. 4). The sole felsic sample M1.1 is classified as an trachy-dacite (Fig. 3) with high Al_2O_3 (16 wt.%), very low CaO and MgO concentrations (Table 1), and a slightly sodic character (Na_2O/K_2O = 1.3; K_2O = 4.1 wt.%).

Because of the relatively small number of samples and their limited range of compositions (excepting felsic sample M1.1), we do not present a range of binary plots for major elements and silica.

4.3. Trace element geochemistry

The basanites have high Ni (250-300 ppm) and Cr (300-400 ppm), mostly high Sr (>2000 ppm) and Ba (1100-1600 ppm) concentrations, along with low Rb (<60 ppm). Concentrations of Sc are largely below the limit of detection (<20 ppm). A single basanite sample M2.3 has higher Ba and Rb and lower Sr concentrations relative to the others, but the nephelinite looks similar to the basanites in terms of LILE concentrations. The basanites and nephelinite have extremely high LREE (light REE) concentrations around 100-600 times chondrite, and steep REE patterns with much lower HREE (heavy REE) concentrations at 10-20 times chondrite and no Eu anomalies (Fig. 4a). They have negative primitive mantle-normalised Rb, K, Nb-Ta, Zr-Hf, and Ti anomalies, with the exception of M2.3 which has a positive Rb and small negative Sr anomaly (Fig. 4b). The nephelinite, with the exception of a

smaller negative K anomaly, is identical on the primitive mantle plot to the basanites. The alkali basalts have slightly lower LREE and MREE concentrations than the basanites, resulting in a slightly less sloped REE pattern compared to the latter (Fig. 4a). Although the alkali basalts also have slightly lower overall LILE and HFSE concentrations compared to the basanites, they have a similar primitive mantle-normalised pattern with negative Rb, K, Nb-Ta, Zr-Hf, and Ti anomalies (Fig. 4b).

The dacite has extremely low Ni, Cr, and Sc concentrations, below the limits of detection. Overall, it contains moderate to high abundances of LILE (1200 ppm Ba, 200 ppm Rb, 47 ppm Th) relative to the mafic rocks, but much lower Sr (800 ppm). The chondrite-normalised (CN) REE pattern for the dacite is concave-up (Dy/Yb_{CN} <1) with the HREE concentrations around 10 times chondrite, and the sample is strongly enriched in the LREE relative to the HREE, with a small negative Eu anomaly (Fig. 4a). Relative to the surrounding REE, the rhyolite has negative primitive mantle-normalised K, Nb-Ta, P, and Ti anomalies and positive spikes at Rb and Th (Fig. 4b). Overall, this sample resembles high-Al, low Mg adakite suites (Defant and Drummond, 1990), although the significance of this association will be discussed later.

4.4. Radiogenic isotope geochemistry

The basanites and alkali basalts have almost identical measured $^{143}Nd/^{144}Nd$ and $^{87}Sr/^{86}Sr$ isotope ratios to one another (Table 2; Fig. 5). Results overall are OIB-like, with compositions very similar to the isolated stratovolcano Mt. Damavand in the Alborz Mountains to the north of the plateau (Davidson et al., 2004), and more depleted in terms of $^{87}Sr/^{86}Sr$ compared to other recent isolated northwest Iranian centres such as at Qorveh and Bijar (200 km to the southeast in Kurdistan Province; Allen et al., 2013), (Fig. 5). The dacite

has a more enriched $^{87}Sr/^{86}Sr$ isotope signature, very slightly closer to upper crustal compositions, but also identical to the mafic Qorveh and Bijar centres. Although only a small number of analyses have been conducted, there is no evidence of a trend in the data for the mafic rocks towards any typical mantle end member compositions such as HIMU, EMI, or EMII, or towards bulk continental crust which typically has enriched $^{143}Nd/^{144}Nd$ and $^{87}Sr/^{86}Sr$ characteristics.

5. Discussion

5.1. Extent of crustal contamination

Overall, the mafic rocks are isotopically homogeneous, showing none of the variability that might be associated with crustal contamination, and have low $^{87}Sr/^{86}Sr$ isotope ratios. In particular there is no change in $^{87}Sr/^{86}Sr$ between the basanites and alkali basalts (Fig. 5). Similarly, all samples have high Mg# (60-70) and are silica under-saturated, both results inconsistent with extensive crustal interaction. Negative Zr-Hf anomalies on normalised plots are also atypical of addition of crustal melts (Fig. 4; Pearce and Peate, 1995). Also, crustal contamination can alter key trace element ratios, but there is no difference in Zr/Hf ratios between the basanites and alkali basalts (Fig. 6a). In contrast, Nb/Ta ratios are slightly lower (18.5-19.0) in the alkali basalts, but we cannot clearly define a common trend between these ratios which may be associated with a crustal component (Fig.6a). The abundances of most incompatible trace elements are far higher than typical continental crust (Taylor and McLennan, 1985), which rules out simple mixing of a primitive magma and crust to produce the observed characteristics (Fig. 6b).

It is most likely that the prominent negative Nb-Ta and Ti anomalies in the mafic rocks (Fig. 4b), which are sometimes associated with crustal contamination, are instead an intrinsic characteristic of the mantle source region. As noted above, the overall abundances of incompatible trace elements are far higher than can be explained by mixing of a primitive magma with typical continental crust, or any likely local contaminant. However, a small (few %) admixture of sediment or other felsic continental crust into the mantle source region is capable of imparting a subduction zone signature to derived melts (e.g. Guo et al., 2006; Allen et al., 2013). There is a caveat that the crustal component must not be so large as to bring the Sr-Nd isotopic values significantly out of the depleted quadrant, although this effect is minimised if the crustal addition itself possesses a relatively depleted signal. Juvenile, Gondwanan (Pan-African) basement or sediments derived thereof may have such a signature, although studies are few at present for the Tethyan subduction and collision system (e.g. Prelevic et al., 2008).

Overall, we conclude therefore that crustal contamination has not taken place on a significant scale, and that elemental characteristics of the mafic lavas are a product of the melting conditions, source mineralogy, and any trace element signatures imparted by subduction processes beneath the region. On the other hand, the single dacite has a higher $^{87}Sr/^{86}Sr$ and slightly lower $^{143}Nd/^{144}Nd$ than the other samples, which may be consistent with a small proportion of crustal contamination (Fig. 5).

5.2. Mantle source and partial melting characteristics of the mafic rocks

5.2.1. Composition and mineralogy of the mantle source

The first topic that we wish to address in this section is the likely make-up of the mantle source of these mafic, alkaline rocks. Firstly, the extremely high incompatible element concentrations in these mafic rocks (Fig. 4b) mean that the mantle source was likely to have been very fertile and/or melted to only a very small degree. Steep REE patterns and fractionation of the HREE indicate that melting took place in the presence of residual garnet, but it seems unlikely that these rocks were generated by melting of a simple garnet peridotite - at small degrees of melting, the source of any melt will most likely be elementally-enriched patches of mantle, or networks of metasomatic veins (Menzies and Murthy, 1980, Wass and Rogers, 1980). We will deal with the mineralogical characteristics of these potential sources in the next section.

Overall, the negative HFSE anomalies on normalised plots (Fig. 4b), and enrichment in the LILE such as Th (Fig. 6b) are taken to imply that the mantle source, whatever its bulk mineralogy, has been influenced at one time or another by subduction-related fluids and/or melts. The negative Nb-Ta anomaly, more simply expressed by high La/Nb ratios of 2-3 (Fig. 6c), is commonly interpreted to result from residual rutile in the subducting slab (e.g. Reagan and Gill, 1989).

It is interesting to note that there is variation in La/Nb ratios between the alkali basalts (La/Nb = 2) and the basanites (La/Nb = 3) is unusual in rocks that overall appear to be co-eval, with overlapping isotopic characteristics (Fig. 6c). Most centres within the collision zone show more uniform La/Nb within individual centres (see Allen et al., 2013, for a more detailed version of Fig. 6c), so varying ratios may be caused by the very low degrees of partial melting required to form these incompatible element-enriched rocks. Rutile is not normally stable in mantle peridotite (Ionov and Hoffman, 1995), but is common in metasomatic veins in the mantle, so residual rutile in the latter may provide an alternative

source of some of the subduction-like HFSE characteristics of the Mahabad lavas, and indeed the varying La/Nb ratios. Allen et al. (2013) argue for contemporaneous melting of rutile-bearing and rutile-free mantle lithologies in the production of high La/Nb arc-like, and low La/Nb OIB-like, alkaline mafic rocks, respectively, from Kurdistan province (Fig. 1). The Kurdistan lavas, along with the stratovolcano Damavand in the Alborz (Fig. 1), are the only other recent centres in the collision zone with similarly variable and high La/Nb to Mahabad (Liotard et al., 2008; Mirnejad et al., 2010; Allen et al., 2013).

Within our sample set however, the key differences between the basanites and alkali basalts, the potassic basanite, and the nephelinite, are their relative concentrations of LREE, LILE and K_2O (Fig. 4). The alkali basalts contain lower concentrations of the REE, and in particular the LREE, compared to the majority of basanites. They also contain lower P_2O_5, HFSE, Sr, Th, and Ba, but higher K_2O relative to the basanites. With the exception of K_2O concentrations relative to other elements, most elemental ratios such as those between the LILE are comparable between the basanites and alkali basalts. The fact that most incompatible element concentrations are simply lower in the alkali basalts suggests that these are the product of greater degrees of partial melting compared to the basanites. Incompatible element ratios sensitive to the degree of partial melting, such as Nb/Yb, and La/Yb, are higher in the basanites (Fig. 6d), corroborating this hypothesis. The higher proportion of K_2O in the alkali basalts may be controlled by a slightly greater proportion of a K_2O-bearing mineral such as phlogopite (mica) or K-richerite (amphibole) in the mantle source (Fig. 6e). A slightly more hydrated, and thus phlogopite ± amphibole-rich mantle source compared to that for the basanites would be more fertile and liable to melt to a higher degree to produce the alkali basalts.

The main differences between the single nephelinite and the basanites are the abundances of K_2O, which is higher in the nephelinite; SiO_2, which is lower by 2 wt.%; and CaO, which is the highest of all the samples (Table 1). Other elemental concentrations and ratios are identical. The simplest interpretation is that the nephelinite has slightly different proportions of olivine and clinopyroxene relative to the basanites, but also that the melt mode happened to contain a slightly higher proportion of phlogopite or K-richterite derived from the mantle source.

The most unusual of the rocks is the single basanite, M2.3, with nearly an order of magnitude higher Rb, along with lower Sr and K_2O compared to the other basanites. As with the nephelinite, this single basanite has identical REE and HFSE behaviour to the other samples. These characteristics imply that the degree of melting is not responsible for the differences described, but that a mineralogical control is present – either in the sample itself or in the mantle source region. High Rb/Sr ratios are typically associated with residual phlogopite (Fig. 6e); which would perhaps also explain why the K_2O concentrations in this sample are low.

Hence, although there is little isotopic variation in the sample set overall, at least in terms of Sr-Nd systematics, there are subtleties within the elemental abundances and ratios that point to a strong mineralogical control on melting characteristics of the source region, apparently dominated by the abundance and/or stability of phlogopite. This controlling factor appears to be complemented by a small variation in the degree of melting to explain the occurrence of both basanites and alkali basalts in such a small geographic area.

5.2.2. HFSE fractionation

One distinctive feature of all of these relatively little-evolved rocks is their super-chondritic Zr/Hf (up to 50) and weakly super-chondritic Nb/Ta ratios (up to 21), the former well outside the field of typical MORB or OIB (David et al., 2000; Pfänder et al., 2007) (Fig. 6a). High Zr/Hf ratios in some intraplate settings have been variously attributed to: (a) proportion of residual clinopyroxene and garnet in the mantle source (Dupuy et al., 1992; Pfänder et al., 2007); (b) extensive clinopyroxene and/or titanite or amphibole fractionation, as these minerals have $D_{Zr} < D_{Hf}$ (Lemarchand et al., 1987); or (c) melting under high ρCO_2 conditions (Dupuy et al., 1992).

A modelled fractional crystallisation curve for clinopyroxene shows that high Zr/Hf ratios can only be reached at unrealistically high degrees of fractionation (Fig. 6a). Conversely, the degree of partial melting required to produce such high Zr/Hf ratios would have to be unrealistically small. Extensive fractionation of mafic minerals and/or titanates is obviously at odds with the primitive, high MgO concentrations of most of the sample set. Carbonate metasomatism was suggested by Dupuy et al. (1992) on the basis of the very high Zr/Hf and Nb/Ta ratios of carbonatite magmas, although the process through which carbonate-rich fluids produce HFSE fractionation is not clear. Although it is not certain that carbonate metasomatism has occurred in the source of the Mahabad lavas, it may be pertinent that they contain rather high CaO (11-15 wt.%), elevated Ba and Sr concentrations, negative Zr-Hf anomalies, and low Ti/Eu ratios - all features recognised in rocks derived from carbonated mantle sources (Ionov et al. 1993; Rudnick et al., 1993).

Garnet in the mantle source is also a plausible explanation for the high Zr/Hf ratios, given that the high LREE/HREE of the samples strongly suggests melting in the presence of garnet. However, Pfänder et al. (2007) concluded that residual garnet would only fractionate Nb and Ta from each other if the source was depleted, with a low initial Zr/Hf (Fig. 6a) -

most likely implying that residual rutile at the point of partial melting is most likely to be responsible for the high Nb/Ta ratios of these lavas (e.g. Foley et al., 2002).

5.2.3. Depth and degree of partial melting

The requirement for melting in the garnet stability field implies melting beneath the garnet-spinel transition zone which may lie at approximately 85 km depth for fertile peridotite (Robinson and Wood, 1998). In Figure 7, we show simple non-modal batch melting curves for two fertile lherzolite sources, with either garnet or spinel present (modelling parameters can be found in Allen et al., in press). We have used the M-HREE to avoid complications judging initial concentrations of LREE and LILE, elements which may be affected by metasomatic processes and the presence of hydrous phases such as phlogopite. This modelling produces results with the correct ratios of the MREE/HREE for our samples, confirming a likely garnet peridotite source for both basanites and alkali basalts, with the alkali basalts having the higher degrees of melting.

However, the REE abundances in typical mantle peridotites are far too low to produce the high abundances in these little-evolved rocks - indicating, as discussed in Section 5.2.1, that magmatism at Mahabad came from a far more fertile source than modelled here (e.g. Fig. 6b). The inferred degree of melting (~10-20%) in our model is as high as beneath mid-ocean ridges or island arcs (Pearce and Stern, 2006), and is highly unlikely given the incompatible element-enriched signature and small volume of the erupted lavas. Therefore this simple modelling serves to confirm that melting of sources such as metasomatic veins or eclogite within the lithospheric mantle are most likely to be responsible for magmatism at Mahabad (e.g. Foley, 1992; Chalot-Prat and Boullier, 1997; Trua et al., 1998; Pilet et al, 2008). Such veins can also contain hydrous phases such as amphibole and phlogopite. We suspect that for

the sodic rocks, phlogopite may not have been present at all during melting; whereas for M2.4 and the alkali basalts, the latter forming at higher degrees of melting, phlogopite was present, thus contributing to higher K_2O in those erupted lavas (e.g. Comin-Chiaramonte et al., 1997).

It is interesting to note that for samples across the Zagros section of the Turkish-Iranian plateau, the oldest dated rocks from the Late Miocene onwards are the most potassic (e.g. east of Lake Urumieh in NW Iran) (Chiu et al., in press), whereas the youngest are mostly highly sodic (Allen et al., 2013); so we speculate that the first melts during this phase of the collision are derived from the most fertile, hydrated lithosphere, rich in phlogopite and capable of melting to moderate degrees (perhaps akin to our alkali basalts). Later on as continental collision progresses, less subduction-related fluid and less hydrous phases are available to aid melting, and thus the melt fraction becomes much smaller, and the melt itself becomes more sodic due to the loss of phlogopite from the lithospheric mantle (c.f. our basanites). Unfortunately, the basanites and alkali basalts are from separate sets of incised flows (Fig. 2) which means we cannot judge their relative ages.

5.3. Exploring the causes of melting

Many models of syn-collisional magmatism within the Turkish-Iranian Plateau equate the Pliocene-Quaternary flare-up to break-off of the southern Neo-Tethyan slab beneath the Bitlis-Zagros suture, and/or delamination of part of the lower lithosphere (Pearce et al., 1990, Keskin, 2003). We sum up models that we think may apply to Mahabad in Figure 8. Geophysical investigations appear to reveal a shallow lithosphere (<50 km) beneath eastern Anatolia, Armenia, and NW Iran, consistent with slab break-off or lithospheric delamination (Zor, 2003; Angus et al., 2006). In such settings, a combination of decompression and asthenospheric heat transfer into the lithospheric mantle is thought to trigger partial melting.

However, recent work implies that there is a significant (>150 km) thickness of lithosphere under much of the collision zone further east, including the Mahabad region (Priestley et al., 2012). This constraint makes it hard to apply either the slab break-off or the delamination model.

There are other possibilities which may apply to some of the Pliocene-Quaternary magmatism occurring here and in other regions of thick lithosphere, such as Kurdistan. Thickening of the lithosphere during the on-going convergence of Arabia and Eurasia will result in compression of sections of the upper mantle to deeper depths than they first stabilised. In such a regime, any hydrous phases such as amphibole or phlogopite may be forced to cross the boundary of their stability fields. Thus these minerals will break down to more stable phases and release water which will thus locally reduce the mantle solidus at the relevant depth. In the case of pargasitic amphibole, breakdown and fluid release occurs at approximately 90 km (Green, 1973). Kushiro et al. (1968) and Sato et al. (1997) demonstrated that phlogopite can break down to form garnet + fluid ± silicate melt at depths of 150-200 km - similar to the inferred depth of the continental lithosphere beneath Mahabad. The breakdown of hydrous phases was one of the many possibilities considered, and ultimately dismissed, by Pearce et al. (1990) for forming the Pliocene-Quaternary volcanics of eastern Anatolia, where we now understand that the lithosphere is unusually thin. However, the model has been revived by Allen et al. (2013) for Quaternary lavas in Kurdistan Province around 200 km along-strike to the southeast of Mahabad. The key constraints on such a model are the timing of lithospheric thickening, and whether or not small volume melts, once formed, will merely freeze in the process of metasomatising the overlying lithospheric mantle, or if they can be efficiently extracted from their source due to localised extension in the overlying plate.

A further geodynamic scenario that may influence partial melting is debated in the literature; that is, the extent to which the Arabian passive margin and any associated sediments have been underthrust beneath the Eurasian margin (e.g. McQuarrie and van Hinsbergen, 2013). It may be possible that Arabian crust is effectively 'subducting' beneath Iranian lithospheric mantle, and thus inducing, or aiding, partial melting of the Iranian mantle by dewatering of hydrated crust (Allen et al., 2013). Specifically Paul et al. (2010) consider that the leading edge of the Arabian continental crust is underthrust beneath the Zagros to a distance of approximately 140 km from the Zagros suture in the centre of the range, and around 250 km in the north. Mahabad, approximately 150 km north-east of the Main Recent Fault in the Zagros, therefore is likely to overlie a region of thickened lithosphere consisting of both Eurasian crust and mantle lithosphere underlain by the subducted Arabian passive margin at depths of around 100 km.

The significance is uncertain, but we note that the Mahabad magmatism also occurs above a region with a pronounced lithospheric thickness gradient (Priestley et al., 2012). The process of edge-driven convection, where lithospheric thickness gradients influence local asthenospheric convection patterns, producing thermal perturbations leading to partial melting (e.g. King and Anderson, 1998) has been linked to magma generation in other settings, such as the Atlas Mountains of Morocco (Missenard and Cadoux, 2012). Around the Zagros Mountains, there is no clear spatial pattern of magmatism orthogonal to the thickness contours of Priestley et al. (2012) (Fig. 1), but we suggest that localised asthenospheric convection be further investigated as a way of heating and/or destabilising the lithospheric mantle beneath the Zagros. If minerals such as phlogopite are 'on the cusp' of breaking down at ~150-200 km, then any thermal perturbation induced by convection of the underlying asthenosphere may be sufficient to induce partial melting of the lowermost lithosphere.

5.4. Origin of the felsic sample

The single felsic sample fits many of the criteria for high-silica adakites (Defant and Drummond, 1990), including high SiO_2, very low MgO, Ni, Cr, high Sr/Y, La/Yb, and moderately low Y and Yb concentrations (Table 1). We do not, however, follow the view taken by Jahangiri (2007) and Omrani et al. (2008) that occurrences of adakites in the Turkish-Iranian Plateau are necessarily related to melting of the Neo-Tethyan slab, akin to early models such as those of Defant and Drummond (1990) and Peacock et al. (1994). Firstly, it has been demonstrated that adakitic melts may be generated by other processes, such as melting of the lower crust, recently underplated or otherwise (Atherton and Petford, 1993; Petford and Gallagher, 2001), or differentiation processes involving mafic arc magmas at various pressures (Macpherson et al., 2006; Castillo, 2012; Richards et al., 2012).

Firstly, at Mahabad, the age of the felsic rocks is not precisely known, but there is no evidence from seismicity that an active subduction zone involving oceanic crust is present beneath Mahabad (or indeed anywhere west of the Makran accretionary complex in southeast Iran). The felsic centre postdates units such as the Miocene Qom Formation, that themselves postdate initial collision. Secondly, the mafic volcanics in this study show little clear sign of slab melt metasomatism. The study of Omrani et al. (2008) was based on 19 samples taken from Anar, around 1000 km south-east of Mahabad within the Urumieh-Dokhtar zone. U-Pb zircon dating by Chiu et al. (in press) indicates an age of ~10-6 Ma for these rocks. Clear trends between Sr-Y and SiO_2 concentrations, such that the least evolved samples from Anar have calc-alkaline, not adakitic chemistries, imply that much of the 'adakite' signature was generated during fractional crystallisation, probably involving amphibole and plagioclase at shallow depths. Richards et al. (2012) noted that suppression of plagioclase fractionation in hydrated arc-like magmas is a process that may lead to the generation of adakitic signatures

such as high Sr/Y ratios. Indeed, there is an increasing body of opinion that melting of amphibolitised or eclogitised basalt in the subducting slab may only be relevant to a small number of cases (Peacock et al., 1994; Macpherson et al., 2006; Castillo, 2012, Richards et al., 2012). The Anar adakites and associated mafic magmas, presumed to be of a similar age, are also isotopically identical to one another (Omrani et al., 2008), indicating that they may have a similar source, rather than one being derived from the slab and one from the fossil mantle wedge.

We must shed caution on any firm interpretation for the origin of the felsic rocks at Kuh-e-Sultan, especially having only analysed one sample. It is possible that this felsic melt originated by fractional crystallisation of a mafic hydrous magma, with a small amount of crustal contamination being responsible for the slightly more enriched composition of the dacite relative to the mafic rocks (Fig. 6). The U-shaped REE profile is consistent with fractionation of amphibole during magmatic evolution (Davidson et al., in press), and large 'spikes' in those LILE incompatible in amphibole (Rb, Th) are also present on the primitive mantle-normalised plot (Fig. 5). However, we cannot arbitrarily rule out melting of a stalled Tethyan slab, or of isotopically depleted lower crust, hence further geophysical and geochemical investigation is necessary.

5.5. Wider implications of this work

As a final comment, we note that young (<10 Ma) magmatism is a ubiquitous feature across the Arabia-Eurasia collision zone, in Turkey, the Greater and Lesser Caucasus, and Iran, a region of highly variable lithospheric thickness and indeed tectonic strain (Fig. 1). Geochemical analyses of these rocks give results ranging from OIB-like to both incompatible element-enriched and depleted arc-like signatures (Pearce et al., 1990; Allen et al., 2013), and

are taken to reflect a variety of lithospheric and asthenospheric mantle sources, along with varying degrees of partial melting and crustal contamination. This heterogeneity implies that there is no single geodynamic trigger for magmatism in orogenic plateaus.

6. Conclusions

We conclude that late Cenozoic mafic magmatism in the region of Mahabad, NW Iran, is derived by small degrees of partial melting of veined mantle lithosphere in the garnet stability field. The "arc-like" signature in these rocks (e.g. La/Nb = 2 to 3) may be inherited from metasomatism by melts/fluids derived from subducted Neo-Tethyan oceanic crust and/or the Arabian plate passive margin. The precise trigger for melting is unclear; popular models of lithosphere delamination and oceanic slab break-off are difficult to apply in a region underlain by lithosphere that is ~150 km thick at the time of melting (Priestley et al., 2012). Three factors may be important in the generation of the magmatism: i) the breakdown of phlogopite and/or amphibole and other hydrous minerals which can induce partial melting during lithospheric thickening; ii) the pronounced lithospheric thickness gradient across northwestern Iran and eastern Anatolia, from ~250 km to <100 km, and iii) the extent to which Arabian continental material has subducted beneath the Eurasian margin and the high Turkish-Iranian Plateau.

Acknowledgments

We thank the Geological Survey of Iran for their longstanding support of our research. Nick Marsh, Geoff Nowell and Chris Ottley aided isotopic and elemental analysis. The project was funded by the Natural Environment Research Council Standard Grant "Orogenic Plateau Magmatism" [NE/H021620/1].

References

Ahmadzadeh, G., Jahangiri, A., Lentz, D., Mojtahedi, M., 2010. Petrogenesis of Plio-Quaternary post-collisional ultrapotassic volcanism in NW of Marand, NW Iran. Journal of Asian Earth Sciences 39, 37-50.

Allen, M.B., Armstrong, H.A., 2008. Arabia-Eurasia collision and the forcing of mid Cenozoic global cooling. Palaeogeography, Palaeoclimatology, Palaeoecology 265, 52-58.

Allen, M.B., Kheirkhah, M., Emami, M.H., Jones, S.J., 2011a. Right-lateral shear across Iran and kinematic change in the Arabia-Eurasia collision zone. Geophysical Journal International 184, 555-574.

Allen, M.B., Mark, D.F., Kheirkhah, M., Barfod, D., Emami, M.H., Saville, C., 2011b. 40Ar/39Ar dating of Quaternary lavas in northwest Iran: constraints on the landscape evolution and incision rates of the Turkish-Iranian plateau. Geophysical Journal International 185, 1175-1188.

Allen, M.B., Kheirkhah, M., Neill, I., Emami, M., McLeod, C.L., 2013. Generation of arc and within-plate chemical signatures in collision zone magmatism: Quaternary lavas from Kurdistan province, Iran. Journal of Petrology, in press, doi:10.1093/petrology/egs090.

Angus, D.A., Wilson, D.C., Sandvol, E., Ni, J.F., 2006. Lithospheric structure of the Arabian and Eurasian collision zone in eastern Turkey from S-wave receiver functions. Geophysical Journal International 166, 1335-1346.

Atherton, M.P., Petford, N., 1993. Generation of sodium-rich magmas from newly underplated basaltic crust. Nature 362, 144-146.

Boccaletti, M., Innocenti, F., Manetti, P., Mazzuoli, R., Motamed, A., Pasquare, G., Radicatidi Brozolo, F., Amin Sobhani, E., 1976. Neogene and Quaternary volcanism of the Bijar area (Western Iran). Bulletin of Volcanology 40, 122-132.

Castillo, P.R., 2012. Adakite petrogenesis. Lithos 134-135, 304-316.

Chalot-Prat, F., Boullier, A.-M., 1997. Metasomatism in the subcontinental mantle beneath the eastern Carpathians (Romania): new evidence from trace element geochemistry. Contributions to Mineralogy and Petrology, 129, 284-307.

Chiu, H.-Y., Chung, S.-L., Zarrinkoub, M.H., Mohammadi, S.S., Khatib, M.M., Iizuka, Y., 2013. Zircon U-Pb age constraints from Iran on the magmatic evolution related to Neo-Tethyan subduction and the Zagros Orogeny. Lithos, in press, doi:10.1016/j.lithos.2013.01.006.

Chung, S.-L., Chu, M.-F., Zhang, Y., Xie, Y., Lo, C.-H., Lee, T.-Y., Lan, C.-Y., Li, X., Zhang, Q., Wang, Y., 2005. Tibetan tectonic evolution inferred from spatial and temporal variations in post-collisional magmatism. Earth-Science Reviews 68, 173-196.

Comin-Chiaramonte, P., Cundari, A., Piccirillo, E.M., Gomes, C.B., Castorina, F., Censi, P., De Min, A., Marzoli, A., Speziale, S., Velázquez, V.F., 1997. Potassic and sodic igneous

rocks from Eastern Paraguay: their origin from the lithospheric mantle and genetic relationships with the associated Paraná flood tholeiites. Journal of Petrology 38, 495-528.

David, K., Schiano, P., Allégre, C., 2000. Assessment of the Zr/Hf fractionation in oceanic basalts and continental material during petrogenetic processes. Earth and Planetary Science Letters 178, 285-301.

Davidson, J.P., Hassanzadeh, J., Berzins, R., Stockli, D.F., Bashukooh, B., Turrin, B., Pandamouz, A., 2004. The geology of Damavand volcano, Alborz Mountains, northern Iran. Geological Society of America Bulletin 116, 16-29.

Davidson, J.P., Turner, S., Plank, T., 2013. Dy/Dy*: Variations arising from mantle sources and petrogenetic processes. Journal of Petrology, in press, doi:10.1093/petrology/egs076.

Defant, M.J., Drummond, M.S., 1990. Derivation of some modern arc magmas by melting of young subducted lithosphere. Nature 347, 662-665.

Dilek, Y., Imamverdiyev, N., Altunkaynak, S., 2010. Geochemistry and tectonics of Cenozoic volcanism in the Lesser Caucasus (Azerbaijan) and the peri-Arabian region: collision-induced mantle dynamics and its magmatic fingerprint. International Geology Review 52, 536-578.

Dowall, D.P., Nowell, G.M., Pearson, D.G., 2007. Chemical pre-concentration procedures for high-precision analysis of Hf-Nd-Sr isotopes in geological materials by plasma ionisation multi-collector mass spectrometry (PIMMS) techniques. I. In: Holland, J.G., Tanner, S.D.,

(eds), Plasma Source Mass Spectrometry: Applications and Emerging Technologies. Cambridge, The Royal Society of Chemistry, 321-337.

Dupuy, C., Liotard, J.M., Dostal, J., 1992. Zr/Hf fractionation in intraplate basaltic rocks: Carbonate metasomatism in the mantle source. Geochimica et Cosmochimica Acta 56, 2417-2423.

Eftekhar-Nezhad, J., 1973. Geological map of Mahabad. Geological Survey of Iran Press.

Foley, S., 1992. Vein-plus-wall-rock melting mechanisms in the lithosphere and the origin of potassic alkaline magmas. Lithos 28, 435-453.

Foley, S., Tiepolo, M., Vannucci, R., 2002. Growth of early continental crust controlled by melting of amphibolite in subduction zones. Nature 417, 837-840.

Furman, T, Graham, D., 1999. Erosion of lithospheric mantle beneath the East African Rift system: geochemical evidence from the Kivu volcanic province. Lithos 48, 237-262.

Green, D.H., 1973. Experimental melting studies on a model upper mantle composition at high pressure under water-saturated and water-undersaturated conditions. Earth and Planetary Science Letters 19, 37-53.

Guo, Z.F., Wilson, M., Liu, J.Q., Mao, Q., 2006. Post-collisional, potassic and ultrapotassic magmatism of the northern Tibetan Plateau: Constraints on characteristics of the mantle source, geodynamic setting and uplift mechanisms. Journal of Petrology 47, 1177-1220.

Ionov, D.A., Dupuy, C., O'Reilly, S.Y., Kopylova, M., Genshaft, Y.S., 1993. Carbonated peridotite xenoliths from Spitsbergen: implications for trace element signature of mantle carbonate metasomatism. Earth and Planetary Science Letters 119, 283-297.

Ionov, D.A., Hofmann, A.W., 1995. Na-Ta-rich mantle amphiboles and micas: Implications for subduction-related metasomatic trace element fractionations. Earth and Planetary Science Letters 131, 341-356.

Jackson, J., Haines, A.J., Holt, W.E., 1995. The accommodation of Arabia-Eurasia plate convergence in Iran. Journal of Geophysical Research 100, 15205-15209.

Jahangiri, A., 2007. Post-collisional Miocene adakitic volcanism in NW Iran: Geochemical and geodynamic implications. Journal of Asian Earth Sciences 30, 433-447.

Keskin, M., Pearce, J.A., Mitchell, J.G., 1998. Volcano-stratigraphy and geochemistry of collision-related volcanism on the Erzurum-Kars Plateau, northeastern Turkey. Journal of Volcanology and Geothermal Research 85, 355-404.

Keskin, M., 2003. Magma generation by slab steepening and breakoff beneath and subduction-accretion complex: An alternative model for collision-related volcanism in Eastern Anatolia, Turkey. Geophysical Research Letters 30, 1-4.

Kheirkhah, M., Allen, M.B., Emami, M., 2009. Quaternary syn-collision magmatism from the Iran/Turkey borderlands. Journal of Volcanology and Geothermal Research 182, 1-12.

Kushiro, I., Syono, Y., Akimoto, S., 1968. Stability of phlogopite at high pressures and possible presence of phlogopite in the earth's upper mantle. Earth and Planetary Science Letters 3, 197-203.

Lebedev, V.A., Chernyshev, I.V., Chugaev, A.V., Dudauri, O.Z., Vashakidze, G.T., 2006. K-Ar age and Sr-Nd characteristics of subalkali basalts in the Central Georgian neovolcanic region. Doklady Earth Sciences 408, 657-661.

Lebedev, V.A., Bubnov, S.N., Chernyshev, I.V., Chugaev, A.V., Dudauri, O.Z., Vashakidze, G.T., 2007. Geochronology and genesis of subalkaline basaltic lava rivers at the Dzhavakheti Highland, Lesser Caucasus: K-Ar and Sr-Nd isotopic data. Geochemistry International 45, 211-225.

Lemarchand, F., Benoit, V., Calais, G., 1987. Trace element distribution coefficients in alkaline series. Geochimica et Cosmochimica Acta 51, 1071-1081.

Le Maitre, R.W., 1989. A Classification of Igneous Rocks and Glossary of Terms. Recommendations of the International Union of Geological Sciences Subcommision on the Systematics of Igneous Rocks. Blackwell, Oxford, 193 pp.

Liotard, J.M., Dautria, J.M., Bosch, D., Condomines, M., Mehdizadeh, J., Ritz, J.F., 2008. Origin of the absarokite-banakite association of the Damavand volcano (Iran): trace elements and Sr, Nd, Pb isotope constraints. International Journal of Earth Sciences 97, 89-102.

Macpherson, C.G., Dreher, S.T., Thirlwall, M.F., 2006. Adakites without slab melting: High pressure differentiation of island arc magma, Mindanao, the Philippines. Earth and Planetary Science Letters 243, 581-593.

Mazhari, S.A., Bea, F., Amini, S., Ghalamghash, J., Molina, J.F., Montero, P., Scarrow, J.H., Williams, I.S., 2009. The Eocene bimodal Piranshahr massif of the Sanandaj-Sirjan Zone, NW Iran: a marker of the end of the collision in the Zagros orogen. Journal of the Geological Society 166, 53-69.

McDonough, W.F., Sun, S.-S., 1995. The composition of the Earth. Chemical Geology 120, 223-254.

McQuarrie, N., Stock, J.M., Verdel, C., Wernicke, B., 2003. Cenozoic evolution of Neotethys and implications for the causes of plate motions. Geophysical Research Letters 30, 2036, doi:2010.1029/2003GL017992.

McQuarrie, N., van Hinsbergen, D.J.J., 2013. Retrodeforming the Arabia-Eurasia collision zone: Age of collision versus magnitute of continental subduction. Geology, in press, doi:10.1130/G33691.1

Menzies, M., Murthy, V.R., 1980. Mantle metasomatism as a precursor to the genesis of alkaline magmas - isotopic evidence. American Journal of Science 280, 622-638.

Mirnejad, H., Hassanzadeh, J., Cousens, B.L., Taylor, B.E., 2010. Geochemical evidence for deep mantle melting and lithospheric delamination as the origin of the inland Damavand

volcanic rocks of northern Iran. Journal of Volcanology and Geothermal Research 198, 288-296.

Missenard, Y., Cadoux, A., 2012. Can Moroccan Atlas lithospheric thinning and volcanism be induced by Edge-Driven Convection? Terra Nova 24, 27-33.

Morley, C.K., Kongwung, B., Julapour, A.A., Abdolghafourian, M., Hajian, M., Waples, D., Warren, J., Otterdoom, H., Srisuriyon, K., Kazemi, H., 2009. Structural development of a major late Cenozoic basin and transpressional belt in central Iran: The Central Basin in the Qom-Saveh area. Geosphere 5, 325-362.

Neill, I., Meliksetian, Kh., Allen, M.B., Navasardyan, G., Karapetyan, S. in review. Pliocene-Quaternary volcanic rocks of NW Armenia: magmatism and lithospheric dynamics within and active orogenic plateau. Lithos.

Notsu, K., Fujitani, T., Ui, T., Matsuda, J., Ercan, T., 1995. Geochemical features of collision-related volcanic rocks in central and eastern Anatolia, Turkey. Journal of Volcanology and Geothermal Research 64, 171-191.

Okay, A.I., Zattin, M., Cavazza, W., 2010. Apatite fission-track data for the Miocene Arabia-Eurasia collision. Geology 38, 35-38.

Omrani, J., Agard, P., Whitechurch, H., Benoit, M., Prouteau, G., Jolivet, L., 2008. Arc-magmatism and subduction history beneath the Zagros Mountains, Iran: A new report of adakites and geodynamic consequences. Lithos 106, 380-398.

Pang, K.-N., Chung, S.-L., Zarrinkoub, M.H., Mohammadi, S.S., Yang, H.-M., Chu, C.-H., Lee, H.-Y., Lo, C.-H., 2012. Age, geochemical characteristics and petrogenesis of Late Cenozoic intraplate alkali basalts in the Lut-Sistan region, eastern Iran. Chemical Geology 306-307, 40-53.

Paul, A., Hatzfeld, D., Kaviani, A., Tatar, M., Péquegnat, C., 2010. Seismic imaging of the lithospheric structure of the Zagros mountain belt (Iran). In: Leturmy, P., Robin, C., (eds), Tectonic and Stratigraphic Evolution of Zagros and Makran during the Mesozoic-Cenozoic: Geological Society of London Special Publications 330, 5-18.

Peacock, S.M., Rushmer, T., Thompson, A.B., 1994. Partial melting of subducting oceanic crust. Earth and Planetary Science Letters 121, 227-244.

Pearce, J.A., Bender, J.F., Delong, S.E., Kidd, W.S.F., Low, P.J., Guner, Y., Sargolu, F., Yilmaz, Y., Moorbath, S., Mitchell, J.G., 1990. Genesis of collision volcanism in eastern Anatolia, Turkey. Journal of Volcanology and Geothermal Research 44, 189-229.

Pearce, J.A., Peate, D.W., 1995. Tectonic implications of the composition of volcanic arc magmas. Annual Review of Earth and Planetary Sciences 23, 251-285.

Pearce, J.A., 1996. A users guide to basalt discrimination diagrams. In: Wyman, D.A., (ed), Trace Element Geochemistry of Volcanic Rocks: Applications for Massive Sulphide Exploration. Geological Association of Canada, Short Course Notes 12, 79-113.

Pearce, J.A., Stern, R.J., 2006. Origin of back-arc basin magmas: Trace element and isotope perspectives. Geophysical Monograph Series, American Geophysical Union 166, 63-86.

Peccerillo, R., Taylor, S.R., 1976. Geochemistry of Eocene calc-alkaline volcanic rocks from the Kastamonu area, northern Turkey. Contributions to Mineralogy and Petrology 58, 63-81.

Petford, N., Gallagher, K., 2001. Partial melting of mafic (amphibolitic) lower crust by periodic influx of basaltic magma. Earth and Planetary Science Letters 193, 483-499.

Pfänder, J.A., Münker, C., Stracke, A., Mezger, K., 2007. Na/Ta and Zr/Hf in ocean island basalts - implications for crust-mantle differentiation and the fate of niobium. Earth and Planetary Science Letters 254, 158-172.

Pilet, S., Baker, M.B., Stolper, E.M., 2008. Metasomatized lithosphere and the origin of alkaline lavas. Science 320, 916-919.

Prelevic, D., Foley, S.F., Romer, R.L., Conticelli, S., 2008. Mediterranean Tertiary lamproites derived from multiple source components in postcollisional geodynamics. Geochimica et Cosmochimica Acta 72, 2125-2156.

Priestley, K., McKenzie, D., Barron, J., Tatar, M., Debayle, E., 2012. The Zagros core: Deformation of the continental lithospheric mantle. Geochemistry, Geophysics, Geosystems 13, Q1 1014, doi:/10.1029/2012GC004435.

Reagan, M.K., Gill, J.B., 1989. Co-existing calc-alkaline and high-Niobium basalts from Turrialba volcano, Costa Rica - implications for residual titanates in arc magma sources. Journal of Geophysical Research - Solid Earth and Planets 94, 4619-4633.

Richards, J.P., Spell, T., Rameh, E., Razique, A., Fletcher, T., 2012. High Sr/Y magmas reflect arc maturity, high magmatic water content, and porphyry Cu ± Mo ± Au potential: examples from the Tethyan arcs of central and eastern Iran and western Pakistan. Economic Geology 107, 295-332.

Robinson, J.A.C., Wood, B.J., 1998. The depth of the spinel to garnet transition at the peridotite solius. Earth and Planetary Science Letters 164, 277-284.

Rudnick, R.L., McDonough, W.F., Chappell, B.W., 1993. Carbonatite metasomatism in the northern Tanzanian mantle: petrographic and geochemical characteristics.

Saadat, S., Stern, C.R., 2012. Petrochemistry of a xenolith-bearing Neogene alkali olivine basalt from northeastern Iran. Journal of Volcanology and Geothermal Research 225-266, 13-29.

Sato, S., Katsura, T., Ito, E., 1997. Phase relations of natural phlogopite with and without enstatite up to 8 GPa: implication for mantle metasomatism. Earth and Planetary Science Letters 146, 511-526.

Şengör, A.M.C., Altiner, D., Cin, A., Ustaomer, T., Hsu, K.J., 1988. Origin and assembly of the Tethyside orogenic collage at the expense of Gondwanaland. In: Audley-Charles, M.G., Hallam, A., (eds), Gondwana and Tethys. Geological Society of London Special Publications 37, 119-181.

Shabanian, E., Acocella, V., Gioncada, A., Ghasemi, H., Bellier, O., 2013. Structural control on volcanism in intraplate post collisional settings: Late Cenozoic to Quaternary examples of Iran and Eastern Turkey. Tectonics, in press, doi:10.1029/2011TC003042.

Taylor, S.R., McLennan, S.M., 1985. The continental crust: Its composition and evolution. Blackwell Scientific Publications, 328 pp.

Trua, T., Esperança, S., Mazzuoli, R., 1998. The evolution of the lithospheric mantle along the N. African Plate: geochemical and isotopic evidence from the tholeiitic and alkaline volcanic rocks of the Hyblean plateau, Italy. Contributions to Mineralogy and Petrology 131, 307-322.

Verdel C., Wernicke, B.P., Hassanzadeh, J., Guest, B., 2011. A Paleogene extensional arc flare-up in Iran. Tectonics 30, TC3008, doi:10.1029/2010TC002809.

Vernant, P., Nilforoushan, F., Hatzfeld, D., Abbassi, M., Vigny, C., Masson, F., Nankali, H., Martinod, J., Ashtiani, A., Bayer, R., Tavakoli, F., Chery, J., 2004. Contemporary crustal deformation and plate kinematics in Middle East constraints by GPS measurements in Iran and northern Iran. Geophysical Journal International 157, 381-398.

Vincent, S.J., Allen, M.B., Ismail-Zadeh, A.D., Flecker, R., Foland, K.A., Simmons, M.D., 2005. Insights from the Talysh of Azerbaijan in to the Paleogene evolution of the South Caspian region. Bulletin of the Geological Society of America 117, 1513-1533.

Walker, R.T., Gans, P., Allen, M.B., Jackson, J., Khatib, M., Marsh, N., Zarrinkoub, M., 2009. Late Cenozoic volcanism and rates of active faulting in eastern Iran. Geophysical Journal International 177, 783-805.

Wass, S.Y., Rogers, N.W., 1980. Mantle metasomatism - precursor to continental alkaline volcanism. Geochimica et Cosmochimica Acta 44, 1811-1824.

Yilmaz, Y., Guner, Y., Saroglu, F., 1998. Geology of the Quaternary volcanic centres of the east Anatolia. Journal of Volcanology and Geothermal Research 85, 173-210.

Zor, E., 2008. Tomographic evidence of slab detachment beneath eastern Turkey and the Caucasus. Geophysical Journal International 175, 1273-1282.

Table captions

Table 1. Major and trace element data from Late Cenozoic lavas, Mahabad, Iran. b.d. = below detection; LOI = loss-on-ignition; Mg# = modal magnesium number.

Table 2. Measured Nd-Sr radiogenic isotopes from Late Cenozoic lavas, Mahabad.

Supplementary Item

Supplementary Item A1. Location information for sampled lavas from Mahabad.

Figure captions

Figure 1. (a) Map of the Turkish-Iranian plateau showing locations of Pliocene-Quaternary volcanism. (b) Location of the UDMA and SSZ. (c) Map of the Iranian sector of the plateau with lithospheric thickness contours from Priestley et al. (2012), at a resolution of 30 km.

Figure 2. Map of the Mahabad area showing sampled outcrops.

Figure 3. (a) $Na_2O + K_2O$ vs. SiO_2 classification (Le Maitre, 1989). (b) K_2O vs. SiO_2 classification (Peccarillo and Taylor, 1976).

Figure 4. (a) REE and extended trace element diagrams for Mahabad. Chondrite and Primitive Mantle values are from McDonough and Sun (1995).

Figure 5. Nd-Sr isotope results for Mahabad. Data are also shown from other mafic Plio-Quaternary rocks within the collision zone: Mt. Ararat and Tendürek in Turkey (Pearce et al., 1990; Kheirkhah et al., 2009); south and central Georgia (Lebedev et al., 2006; 2007); NW Armenia (Neill et al., in review); Kurdistan along-strike from Mahabad within the Sanandaj-Sirjan Zone (Allen et al., 2013); minor centres in NW Iran such as Yigit Dagi, Salmas, Siah Chesmeh, and Gonbad (Kheirkhah et al., 2009); and Mt. Damavand, Iran (Davidson et al., 2004; unpublished data).

Figure 6. Trace element ratio plots for Mahabad and including data from other Late Cenozoic centres in the Turkish-Iranian plateau (compiled in Allen et al., 2013 and Neill et al., in review). a) Zr/Hf vs. Nb/Ta showing modelled clinopyroxene fractionation curve (Neill et al., in review) and partial melting curves for garnet peridotites with different starting Zr/Hf ratios

(Pfänder et al., 2007). b) Th/Yb vs. Ta/Yb (Pearce, 1983) indicating LILE enrichment of the Mahabad mafic lavas and overall incompatible element enrichment in excess of typical continental crust (Taylor and McLennan 1985). c) La vs. Nb after Allen et al. (2013). demonstrating the wide range of compositions, from OIB-like to arc-like, displayed by recent small-volume centres such as Damavand and Kurdistan. d) Nb/Yb vs La/Yb. e) Rb/Sr vs. Ba/Rb (after Furman and Graham, 1999) displaying possible control by phlogopite and amphibole on the compositions of some of the mafic rocks from Mahabad.

Figure 7. Partial melting curves for different peridotite types (see Allen et al., 2013, for details of modelling).

Figure 8. Lithospheric cross-section using models of Paul et al. (2010) and Priestley et al. (2012) to demonstrate that melting may be triggered by one or several of the following processes: breakdown of hydrous phases during lithospheric thickening; refertilisation of the source by flux from subducted Arabian crust; asthenospheric convection along the lithospheric gradient presented by the Zagros core. Phase diagram from Green, 1973.

Vitae:

- Monireh Kheirkhah is an Assistant Professor in the Research Institute for Earth Sciences at the Geological Survey of Iran. She works on the geochemistry and geodynamics of the young magmatism of the Arabia-Eurasia collision, on the Turkish Iranian Plateau. Monireh graduated from Tehran University (BSc) and Azad University (PhD).

- Iain Neill is a postdoctoral researcher at Durham University. He uses geochemistry and geochronology to link plate tectonics and magmatism in regions as diverse as the Arabia-Eurasia collision, the Caribbean, and the Scottish Caledonides. Iain has a BSc from The University of St. Andrews and a PhD from Cardiff University.

- Mark Allen is a Reader at Durham University. He works on continental tectonics and magmatism, with a focus on tectonically active regions of Eurasia within the Arabia-Eurasia and India-Eurasia collision zones. He studied at Durham and Leicester Universities for his BSc and PhD, respectively.

- Keivan Agdari works in the Research Institute for Earth Sciences as a petrologist. He graduated from Tehran University (BSc) and the Research Institute for Earth Sciences (MSc). His research interest is the young basic rocks of Iran.

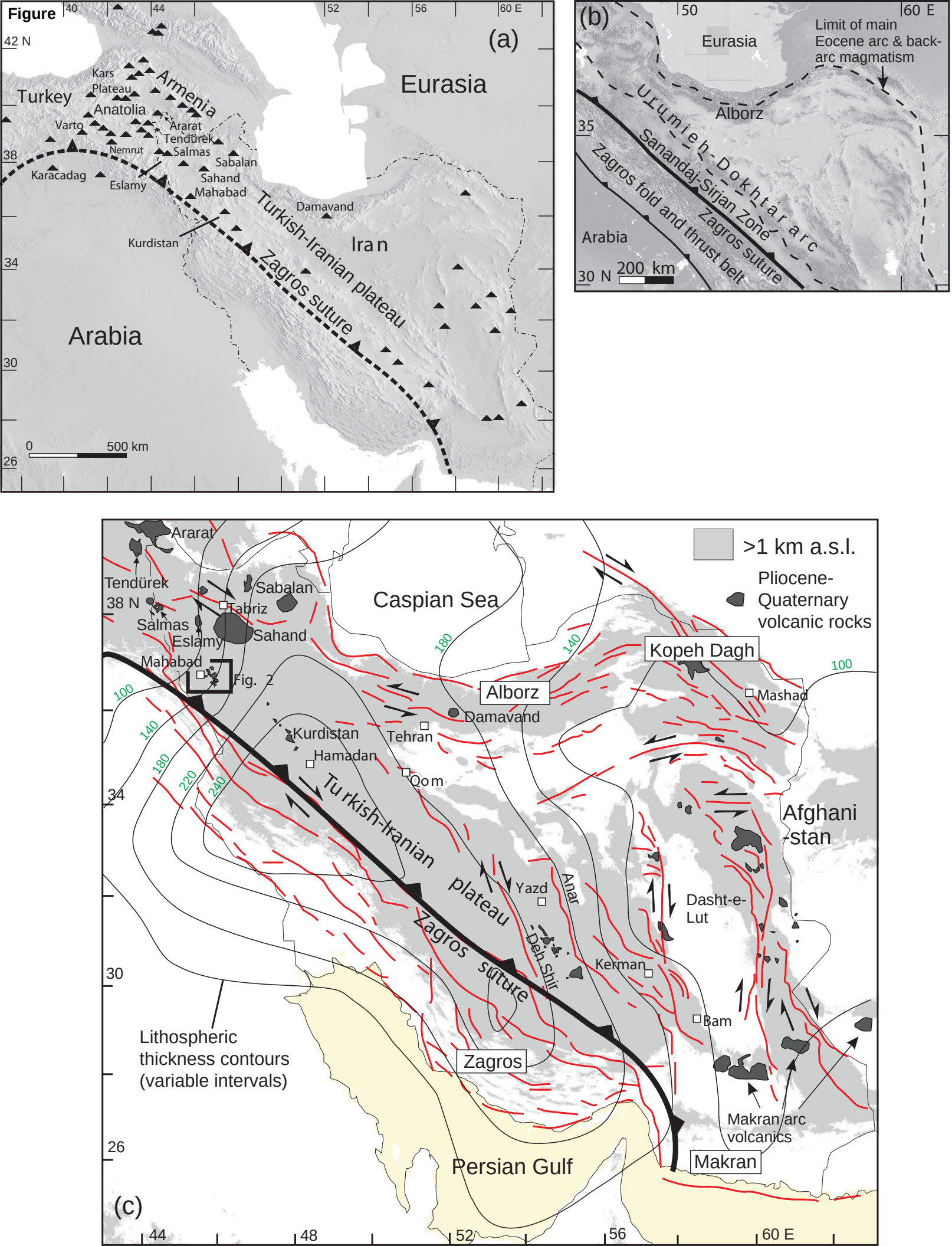
Figure
(a)
Eurasia
Turkey
Armenia
Kars
Plateau
Anatolia
Varto
Ararat
Tendürek
Nemrut
Salmas
Sabalan
Sahand
Karacadag
Eslamy
Mahabad
Damavand
Kurdistan
Iran
Turkish-Iranian plateau
Zagros suture
Arabia
0
500 km
(b)
Eurasia
Limit of main Eocene arc & back-arc magmatism
Alborz
Urumieh-Dokhtar arc
Sanandaj-Sirjan Zone
Zagros suture
Zagros fold and thrust belt
Arabia
200 km
>1 km a.s.l.
Pliocene-Quaternary volcanic rocks
Ararat
Tendürek
Sabalan
Tabriz
Salmas
Eslamy
Sahand
Mahabad
Fig. 2
Caspian Sea
Kopeh Dagh
Alborz
Damavand
Mashad
Kurdistan
Tehran
Hamadan
Qom
Turkish-Iranian plateau
Zagros suture
Yazd
Anar
Deh Shir
Dasht-e-Lut
Afghanistan
Kerman
Bam
Zagros
Makran arc volcanics
Makran
Persian Gulf
Lithospheric thickness contours (variable intervals)
100
140
180
220
240
(c)

Figure 5 isotopes

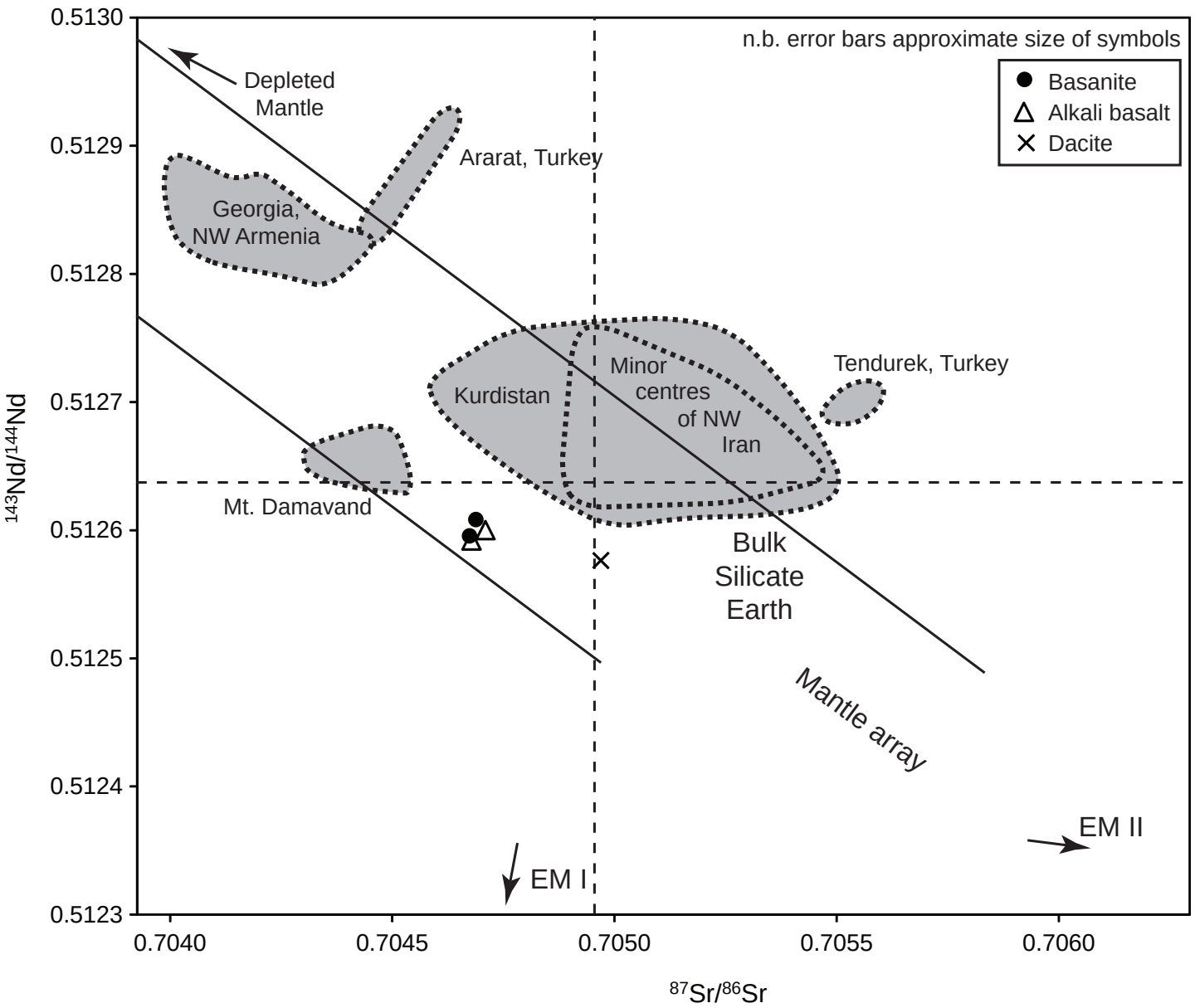

Table 2 isotope results

Table 2. Measured Nd-Sr radiogenic isotopes from Late Cenozoic lavas, Mahabad.

Sample	M3.1	M5.2	M6.1	M7.1	M1.1
Rock	Basanite		Alkali basalt		Dacite
$^{87}Sr/^{86}Sr$	0.704435	0.704415	0.704479	0.704413	0.705100
Error (1σ)	0.000004	0.000004	0.000004	0.000005	0.000005
$^{143}Nd/^{144}Nd$	0.512696	0.512689	0.512682	0.512674	0.512653
Error (1σ)	0.000004	0.000005	0.000004	0.000004	0.000005
εNd (1σ error)	1.13 ± 0.09	0.99 ± 0.10	0.86 ± 0.08	0.70 ± 0.08	0.29 ± 0.09

Supplement A1

Click here to download e-component: Mahabad SupplementA1.docx